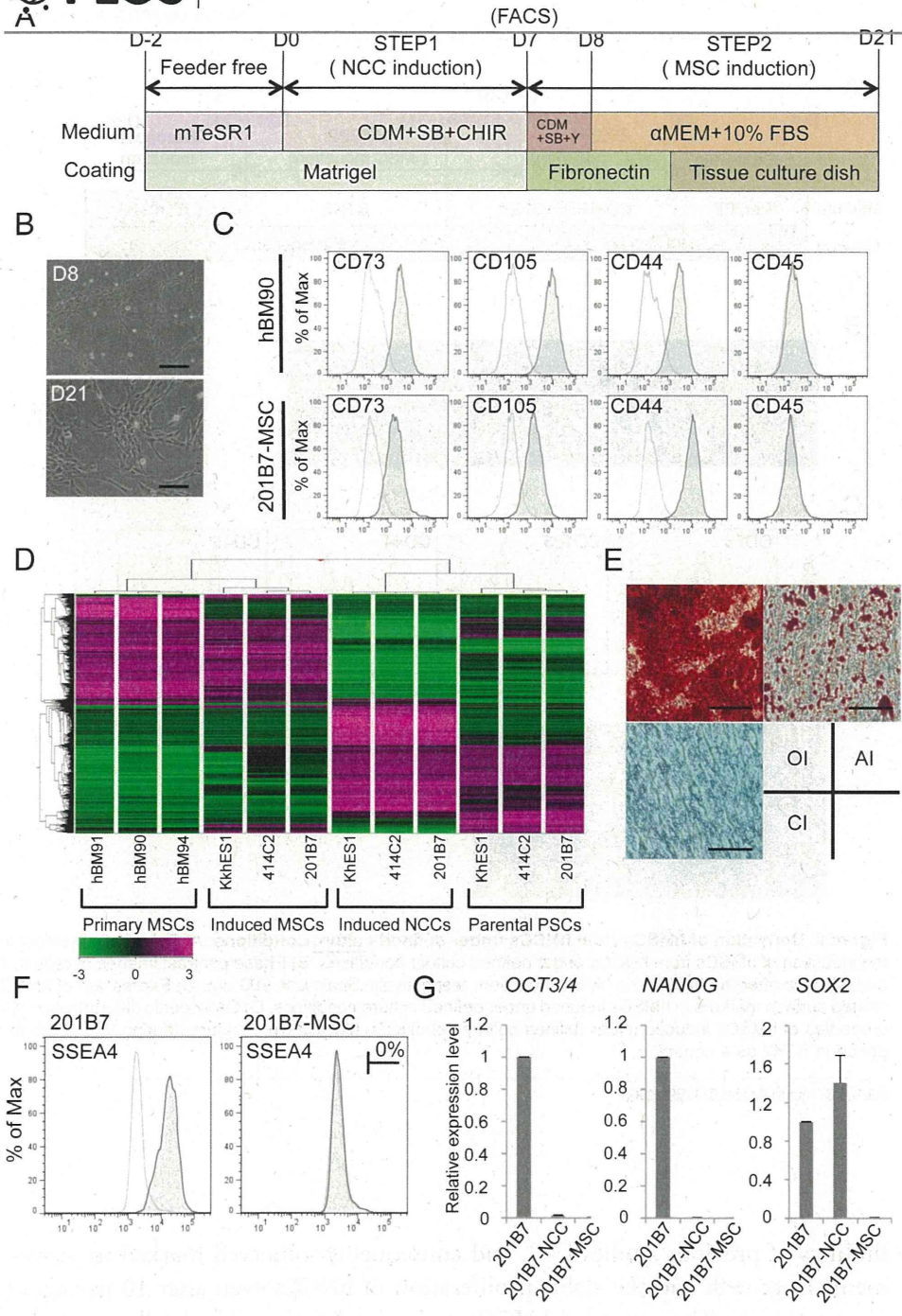

Figure 7. Derivation of hMSCs from hNCCs. A) Schematic protocol for the induction of hMSCs. B) Phase contrast images of cells before (D8) and after (D21) the induction. Scale bar, 200 μm. C) Expression of surface markers in hBM-MSCs (hBM90) and 201B7-derived MSCs (201B7-MSC). D) Hierarchical clustering analyses by genome-wide gene expression profiles. RNAs were extracted from hBM-MSCs (BM90, BM91 and BM94), induced-MSCs, and the corresponding hNCCs and hiPSCs. E) Differentiation properties of induced-MSCs. The induction for osteogenic (OI), chondrogenic (CI), and adipogenic (AI) lineages was performed as described in the Materials and Methods section and evaluated by Alizarin Red staining (OI), Alcian Blue staining (CI), and Oil Red O staining (AI), respectively. Scale bar, 100 μm. F) Population of SSEA4-positive cells. G) The expression levels of pluripotent markers (*OCT3/4*, *NANOG* and *SOX2*) in hPSCs, hNCCs, and hMSCs. Average ± SD. N=3, biological triplicates.

doi:10.1371/journal.pone.0112291.g007

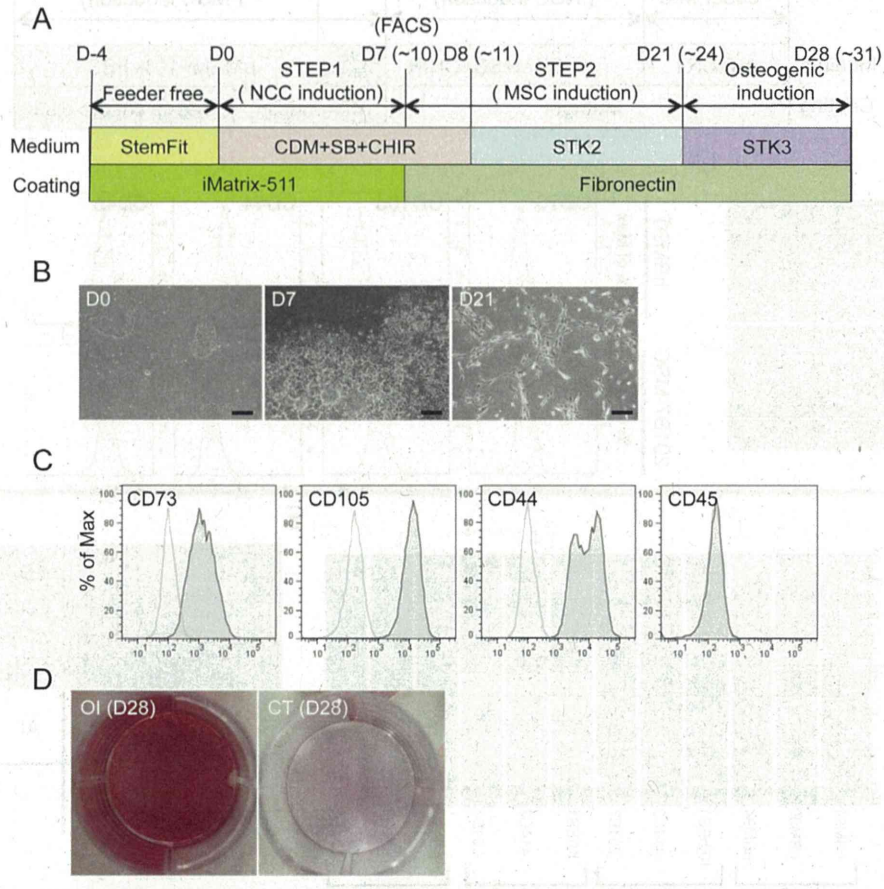

Figure 8. Derivation of hMSCs from hNCCs under defined culture conditions. A) Schematic protocol for the induction of hMSCs from hNCCs under defined culture conditions. B) Phase contrast images of cells 0, 7, and 21 days after the hNCC and hMSC induction, respectively. Scale bar, 200 μm. C) Expression of hMSC-related surface markers in hMSCs induced under defined culture conditions. D) Osteogenic differentiation (OI) properties of hMSCs induced under defined culture conditions. hMSCs were cultured during the induction period in STK2 as a control.

doi:10.1371/journal.pone.0112291.g008

findings of previous studies [33], and consequently observed marked improvements in growth and the stable proliferation of hNCCs even after 10 passages (Figures 3A, B). The expanded hNCCs maintained their original cell morphology and all cells expressing NCC markers, such as TFAP2A (Figure 3C). The global gene expression profiles of hNCCs after prolonged expansion (PN10) were similar to those of early-passage cells (PN0) (Figure S4A and S4B, correlation coefficient =0.96 to 0.98) and markedly different from those of original hPSCs (Figures 3D and S4C).

Modulation of the characteristics of hNCCs by insulin and retinoic acid (RA)

The results of the microarray analyses revealed that induced hNCCs expressed some genes characteristic to cranial NCCs (high for *OTX2* and *DLX1*; low for *HOXA2* and *HOXA3*) (date not shown). A previous study demonstrated that the depletion of insulin from CDM (growth-factor free CDM; hereafter referred to as gfCDM) induced a more anterior neuroectoderm (rostral hypothalamic progenitor-like cells), while retinoic acid (RA) exhibited posteriorizing activity [15]. Therefore, we compared the expression of regional markers in hNCCs cultured with gfCDM, CDM, and CDM with RA (100 nM) (Figure 4A). As expected, the expression of *OTX2*, a marker for mesencephalic NCCs (Figure 4B) [34], was slightly higher under the gfCDM condition than under the CDM condition (Figure 4C). The *DLX1* gene, a marker for first and second branchial arch NCCs (Figure 4B) [35], was expressed in cells cultured under all conditions, and was the highest in CDM with the RA condition (Figure 4C). The expression of the *HOXA2* and *HOXA3* genes, which are markers of the second and third branchial arches, was negligible under the gfCDM and CDM conditions (Figures 4B, C) [36, 37]. Taken together, these results indicated that the regional identities of hNCCs could be modulated by exogenous signals including insulin and RA.

Derivation of peripheral neurons, glia, and melanocytes from hNCCs

We next examined the differentiation potentials of induced hNCCs. Neuronal differentiation was initiated by sphere formation and promoted by culture media containing a mixture of factors (BDNF, GDNF, NGF, and NT-3). Cells expressed β-tubulin and peripherin after 14 days, which indicated differentiation into peripheral neurons (Figure 5A). Further cultivation under the same conditions (4 to 6 weeks) promoted the glial differentiation of hNCCs (Figure 5B).

Melanocytes are well-known derivatives of NCCs. Using a previously described method that included CHIR, EDN3, and BMP4 [15, 38], induced hNCCs expressed microphthalmia-associated transcription factor (*MITF*) and *c-KIT*, markers for melanocytes (Figure 5C). These differentiation properties were compatible with those of NCCs *in vivo*.

Derivation of corneal endothelial cells from hNCCs

Cranial NCCs have been shown to exhibit the ability to differentiate into corneal endothelial cells *in vivo* [39, 40]. Therefore, we examined whether hNCCs grown in gfCDM, which preferentially expressed more anterior NCC markers (Figures 4B, C), could differentiate into cells harboring the characteristics of corneal endothelial cells. When 201B7-derived hNCCs were cultured in the conditioned medium of corneal endothelial cells for twelve days (Figure 6A), cells changed their morphology into that of polygonal corneal endothelial-like cells (

Figure 6B) and started to express the corneal endothelial marker, ZO-1 (Figure 6C). Descemet's membrane is known to consist of collagen type 4 and collagen type 8, which are derived from the corneal endothelium [41]. The mRNA expression of the *COL4A1* and *COL8A1* genes was confirmed in induced endothelial-like cells (Figure 6D). These results strongly suggested that the hNCCs induced in this study possessed the characteristics of cranial NCCs, which exhibit the potential to differentiate into cranial NCC-derived structures.

Derivation of hMSCs from hNCCs

Cranial NCCs also have differentiation properties toward mesenchymal cells, which construct the cranio-facial skeleton, and may be referred as MSCs [3]. In order to derivate hMSCs from hNCCs, the culture medium was changed from that for hNCC to αMEM with 10% FBS (Figure 7A), which we used previously for human bone marrow-derived MSCs (hBM-MSCs) [24]. Through the induction of hMSCs, the expression of *NGFR* and *SOX10* reduced rapidly within 48 hours (PN0) of the medium change, while that of *PAX3* and *TFAP2A* reduced gradually until passage 3 (Figure S5A). Conversely, the expression of MSC markers (*CD73*, *CD105*, and *CD44*) increased rapidly within 48 hours, reached a maximum by passage number 2, and maintained their expression at a level comparable to that in BMMSCs (Figure S5B). These results indicated that the transition from NCCs to MSCs was gradual during passage number three. Cells passaged three times in the medium showed a typical fibroblastic morphology similar to that of hMSCs (Figure 7B), and expressed surface markers for hMSCs (positive for CD73, CD105, and CD44, and negative for CD45) (Figure 7C). Microarray analyses revealed that hNCC-derived MSCs had a global expression pattern similar to that of primary hBM-MSCs (Figure 7D). Differentiation properties toward osteogenic, chondrogenic, and adipogenic lineages are one of the criteria required for MSCs [42], which were clearly confirmed in hNCC-derived MSCs (Figure 7E). FACS analysis showed that there was no SSEA4-positive cells (Figure 7F) and the expression of PSC marker genes was below detectable levels (Figure 7G).

Derivation of osteogenic cells from hiPSCs under defined culture conditions

We determined the feasibility of inducing terminally differentiated cells from iPSCs under defined culture conditions (Figure 8). 987A3 hiPSCs were used as the initial material, which have been generated and maintained under feeder-free and xeno-free conditions [21]. Cells were dissociated into single cells, seeded on iMatrix-coated dishes (0.83–1.35 cells/cm^2), and cultured with StemFit medium for five days. hNCCs were then induced for seven to ten days (Figure 8A). The efficiency of hNCC induction under these conditions was 40.9 ± 5.5% (± SD. N=3, biological triplicate). The induction of hMSCs was performed using CDM for MSCs (STK2) instead of αMEM/10% FBS (Figure 8A). After several passages of hNCCs in STK2, the morphology of cells changed from cuboidal to fibroblastic,

similar to that of hBM-MSCs (Figure 8B). The expression patterns of surface markers were compatible with those of hMSCs (positive for CD73, CD105, and CD44, and negative for CD45) (Figure 8C) and the differentiation properties for osteogenic, chondrogenic, and adipogenic lineages were confirmed when the standard FBS-containing induction medium was used (Figure S6). Osteogenic differentiation was also confirmed using the chemically-defined osteogenic medium (STK3) (Figure 8D). These results indicated that all steps from iPSC to osteogenic cells could be performed under defined culture conditions.

Discussion

In the present study, we developed a simple and efficient induction method for hNCCs from hPSCs. The induction efficiency of this method was high (70–80%) irrespective with the type of hPSC. The induced hNCCs exhibited the cranial NCC characters under maintenance culture conditions, while further treatment with insulin and RA marginally posteriorized hNCCs. Consistent with the expression of cranial NCC markers, induced hNCCs could differentiate into corneal endothelial cells, which is a characteristic of cranial NCCs.

Our protocol was independent of the BMP signal. In our protocol, DMH1, a specific BMP inhibitor, clearly attenuated the induction efficiency of the $p75^{high}$ fraction (Figure S1). This result clearly contradicted the findings of previous studies (no effect [14] or increased efficiency [15]). The marked differences in the findings of these studies may be attributed to the seeding density used at the beginning of induction. The seeding density of our protocol was approximately 2–4 clumps/cm^2 (approximately 20 cells/cm^2), while other studies used 1×10^4 cells/cm^2 [26]. Both CNS and neural crest fates were previously observed when cells were seeded at a low density, while CNS cells primarily formed at a high density [43]. In accordance with these findings, the efficiency of the NCC induction was markedly decreased if clumps were seeded at a higher density (data not shown). The high density of hNCCs may have exaggerated local BMP signaling secreted from the hNCCs themselves. Therefore, we combined high density seeding with the BMP inhibitor treatment; however, the efficiency was still low (data not shown). Based on these results, we could not account for the differences between our protocol and those of previous studies.

In order to compare the hNCCs in this study with those in previous studies, we analyzed gene expression profiles of hNCCs published previously. The comparison of the relative induction levels of NCC specific genes revealed that hNCCs differentiated by our protocol and previous studies showed similarities in some aspects, but overall profiles were different from each other (Figure S3). These results indicated that induction protocols reported in this study and in the previous studies induced different subset of hNCCs.

Induced hNCCs exhibited differentiation properties for multiple cell lineages including peripheral neurons, glial cells, melanocytes, and corneal endothelial cells, and also delivered hMSCs that further differentiated into osteogenic,

chondrogenic, and adipogenic cells. These properties are compatible with NCCs being multipotent stem cells [3]. However, clonal analyses are indispensable for confirming the stemness of induced hNCCs. Previous clonal analyses revealed that 63–65% of the hNCC clones could differentiated into multi-lineage cells positive for markers of neurons, glial cells, and smooth muscle cells [43, 44], suggesting that hNCCs induced from hPSCs were multipotent on the clonal level. Although stemness has yet to be investigated in this study, induced hNCCs in this protocol will be a promising cell source for various types of research.

Human diseases that have been related to the development of hNCCs include Hirschsprung's disease, DiGeorge syndrome, Waardenburg syndrome, Charcot-Marie-tooth disease, Hermansky-Pudlak syndrome, familial dysautonomia, Chediak-Higashi syndrome, and CHARGE syndrome [45, 46]. hNCCs containing the mutations responsible for these diseases can be induced from hiPSCs established from the respective patients; therefore, this will be a powerful tool for creating *in vitro* disease models that can contribute to a more detailed understanding of the pathogenesis of NCC disorders and also to the development of novel therapeutic modalities [15]. In addition, hNCCs have been shown to be the cell-of-origin of some cancers such as neuroblastoma [47], which indicates that hNCCs can be used in *in vitro* transformation experiments. We have already confirmed that the survival rate of freeze-stocked hNCCs was satisfactory and the freeze and thaw process had no impact on the growth and differentiation properties of these cells (data not shown). These are favorable features for a material in research because it is important to use cells of the same quality in order to evaluate reproducibility.

Induced hNCCs-deridatives can also be used for cell therapy. In this regard, hNCC-derived hMSCs will be a very useful material. hMSCs have been used in a wide range of regenerative medicines, and promising results have been reported in some cases [48, 49]. In contrast with the advances reported in clinical applications, many issues related to the biology of hMSCs have yet to be investigated, one of which is the cell-of-origin of hMSCs. hNCCs may be the precursors of hMSCs based on the finding that craniofacial skeletal tissues are derived from NCCs [50]. This has also been supported in lineage tracing experiments using P0-cre mice [51, 52]. Current sources of hMSCs include bone marrow, fat tissue, synovium, and umbilical cord; however, it remains unclear whether NCC-derived cells exist in all of these adult tissues and serve as the source of hMSCs. A comparison between hNCC-derived MSCs and somatic tissue-derived hMSCs may provide more information related to this issue.

One of the limitations of current hMSCs is their limited proliferative activity, which may pose problems in their application to conditions requiring a large amount of cells. This can be overcome if hNCC-derived MSCs are used because hNCCs can be induced from hPSCs, which have unlimited proliferative activity. Two issues are important for this application. One is to be free from infectious substances that may be derived from animal materials. Using iPSCs generated and maintained under feeder-free and xeno-free conditions, we successfully induced hNCCs and hMSCs with minimum animal material (BSA in CDM) (Figure 8A).

Furthermore, we generated terminally differentiated cells (osteogenic cells) from these MSCs under chemically defined media. To the best of our knowledge, this is the first study to demonstrate the induction of osteogenic cells under feeder-free and serum-free conditions from PSCs. The other concern relates to the contamination of undifferentiated cells, particularly parental hPSCs, which may lead to serious conditions such as the formation of malignant tumors [53]. We confirmed that hNCC-derived hMSCs were free from SSEA4-expressing cells and the expression of PSC-marker genes was below detectable levels (Figures 7F, G). Although more precise and meticulous analyses are required to prove the safety of these cells, the results of the present study have provided evidence to promote the use of hNCC-derived hMSCs for cell therapy.

Supporting Information

Figure S1. Effect of the BMP signal on the induction of $p75^{high}$ cells. hiPSCs (201B7) were treated in NCC induction media with BMP4 (10 ng/ml) (A) or DMH1 (10 μM) (B), and the fraction of p75-positive cells was analyzed by FACS. C) Effects of BMP signal inhibitors on the induction of $p75^{high}$ cells. 201B7 cells were treated with each BMP inhibitor at the indicated dosage, and the fraction of p75-positive cells was analyzed by FACS.
doi:10.1371/journal.pone.0112291.s001 (TIFF)

Figure S2. Global comparison of the expressions of genes between PSCs and $p75^{high}$ cells. A) A volcano plot showing the P value for differences in the expression of each gene between the average of PSC lines (H9, KhES1, 414C2, and 201B7) and the average of corresponding $p75^{high}$ cells. A total of 562 entities downregulated and 447 entities upregulated in $p75^{high}$ cells were identified as a differentially expressed gene set. B) Heat map analyses revealed global similarities among hNCCs derived from each PSC line.
doi:10.1371/journal.pone.0112291.s002 (TIFF)

Figure S3. Expression of NCC marker genes in induced NCCs from PSCs. The induction ratio of NCC markers relative to a corresponding pluripotent baseline was demonstrated in each induced NCC. iPS NCCs, GSE44727. WA09_NC_Day11, 45223. Marker genes for each sub-population of NCC were labeled using the indicated colors.
doi:10.1371/journal.pone.0112291.s003 (TIFF)

Figure S4. Comparison of gene expression profiles between hNCCs at different passages by scatter plotting. RNAs were extracted from hNCCs derived from 201B7 (A) and KhES1 (B) at different passages (PN0, PN4 and PN10), and analyzed using microarrays. C) Correlation coefficient analysis was performed using these data.
doi:10.1371/journal.pone.0112291.s004 (TIFF)

Figure S5. The expression of markers for hNCCs and hMSCs in each passage. A gradual transition from hNCCs to hMSCs was observed in hNCC markers (A)

and hMSC markers (B). Average ± SD. N=3, biological triplicates. Regarding BMSCs, cDNA was prepared from the bone marrow stromal cells of four healthy donors (BM25, 26, 34, and 107), and the average was presented as BMSCs in each graph.
doi:10.1371/journal.pone.0112291.s005 (TIFF)

Figure S6. Osteogenic-, chondrogenic-, adipogenic induction from feeder-free hiPSCs through hNCC-derived hMSCs. Differentiation properties of hNCC-MSCs. The induction for osteogenic (OI), chondrogenic (CI), and adipogenic (AI) lineages was performed as described in the Materials and Methods section and evaluated by Alizarin Red staining (OI), Alcian Blue staining (CI), and Oil Red O staining (AI), respectively. Scale bar, 200 μm.
doi:10.1371/journal.pone.0112291.s006 (TIFF)

Table S1. Information of primary antibodies used in this study.
doi:10.1371/journal.pone.0112291.s007 (TIF)

Table S2. Information of PCR primers used in this study.
doi:10.1371/journal.pone.0112291.s008 (TIF)

Acknowledgments

We thank Dr. H. Tanaka for the kind advice and help in the corneal endothelium induction, M. Shibata, K.R. Komatsu, and J. Nakai for their technical assistance, and T. Kato, Y. Jin. S. Tamaki, and S. Hineno for their support during this study.

Author Contributions

Conceived and designed the experiments: MF NK TN MS TO SK MU MI JT. Performed the experiments: MF YN KK KS SN YM TY NO TS MI. Analyzed the data: MF YN KK NK MU TS MI. Contributed reagents/materials/analysis tools: MN TY KU TH. Wrote the paper: MF YN TY MU MI JT.

References

1. **Liu Z, Tang Y, Lu S, Zhou J, Du Z, et al.** (2013) The tumourigenicity of iPS cells and their differentiated derivates. J Cell Mol Med 17: 782–791.
2. **Le Douarin NM, Dupin E** (2003) Multipotentiality of the neural crest. Curr Opin Genet Dev 13: 529–536.
3. **Sauka-Spengler T, Bronner-Fraser M** (2008) A gene regulatory network orchestrates neural crest formation. Nat Rev Mol Cell Biol 9: 557–568.
4. **Kalcheim C, Burstyn-Cohen T** (2005) Early stages of neural crest ontogeny: formation and regulation of cell delamination. Int J Dev Biol 49: 105–116.
5. **Kalcheim C** (2000) Mechanisms of early neural crest development: from cell specification to migration. Int Rev Cytol 200: 143–196.
6. **Vincent SD, Buckingham ME** (2010) How to make a heart: the origin and regulation of cardiac progenitor cells. Curr Top Dev Biol 90: 1–41.

7. **Neirinckx V, Coste C, Rogister B, Wislet-Gendebien S** (2013) Concise review: adult mesenchymal stem cells, adult neural crest stem cells, and therapy of neurological pathologies: a state of play. Stem Cells Transl Med 2: 284–296.

8. **Neirinckx V, Marquet A, Coste C, Rogister B, Wislet-Gendebien S** (2013) Adult bone marrow neural crest stem cells and mesenchymal stem cells are not able to replace lost neurons in acute MPTP-lesioned mice. PLoS One 8: e64723.

9. **Giuliani M, Oudrhiri N, Noman ZM, Vernochet A, Chouaib S, et al.** (2011) Human mesenchymal stem cells derived from induced pluripotent stem cells down-regulate NK-cell cytolytic machinery. Blood 118: 3254–3262.

10. **Villa-Diaz LG, Brown SE, Liu Y, Ross AM, Lahann J, et al.** (2012) Derivation of mesenchymal stem cells from human induced pluripotent stem cells cultured on synthetic substrates. Stem Cells 30: 1174–1181.

11. **Liu Q, Spusta SC, Mi R, Lassiter RN, Stark MR, et al.** (2012) Human neural crest stem cells derived from human ESCs and induced pluripotent stem cells: induction, maintenance, and differentiation into functional schwann cells. Stem Cells Transl Med 1: 266–278.

12. **Chimge NO, Bayarsaihan D** (2010) Generation of neural crest progenitors from human embryonic stem cells. J Exp Zool B Mol Dev Evol 314: 95–103.

13. **Milet C, Monsoro-Burq AH** (2012) Embryonic stem cell strategies to explore neural crest development in human embryos. Dev Biol 366: 96–99.

14. **Menendez L, Yatskievych TA, Antin PB, Dalton S** (2011) Wnt signaling and a Smad pathway blockade direct the differentiation of human pluripotent stem cells to multipotent neural crest cells. Proc Natl Acad Sci U S A 108: 19240–19245.

15. **Mica Y, Lee G, Chambers SM, Tomishima MJ, Studer L** (2013) Modeling neural crest induction, melanocyte specification, and disease-related pigmentation defects in hESCs and patient-specific iPSCs. Cell Rep 3: 1140–1152.

16. **Suemori H, Yasuchika K, Hasegawa K, Fujioka T, Tsuneyoshi N, et al.** (2006) Efficient establishment of human embryonic stem cell lines and long-term maintenance with stable karyotype by enzymatic bulk passage. Biochem Biophys Res Commun 345: 926–932.

17. **Amit M, Carpenter MK, Inokuma MS, Chiu CP, Harris CP, et al.** (2000) Clonally derived human embryonic stem cell lines maintain pluripotency and proliferative potential for prolonged periods of culture. Dev Biol 227: 271–278.

18. **Okita K, Matsumura Y, Sato Y, Okada A, Morizane A, et al.** (2011) A more efficient method to generate integration-free human iPS cells. Nat Methods 8: 409–412.

19. **Takahashi K, Tanabe K, Ohnuki M, Narita M, Ichisaka T, et al.** (2007) Induction of pluripotent stem cells from adult human fibroblasts by defined factors. Cell 131: 861–872.

20. **McMahon AP, Bradley A** (1990) The Wnt-1 (int-1) proto-oncogene is required for development of a large region of the mouse brain. Cell 62: 1073–1085.

21. **Nakagawa M, Taniguchi Y, Senda S, Takizawa N, Ichisaka T, et al.** (2014) A novel efficient feeder-free culture system for the derivation of human induced pluripotent stem cells. Sci Rep 4: 3594.

22. **Nasu A, Ikeya M, Yamamoto T, Watanabe A, Jin Y, et al.** (2013) Genetically matched human iPS cells reveal that propensity for cartilage and bone differentiation differs with clones, not cell type of origin. PLoS One 8: e53771.

23. **Wataya T, Ando S, Muguruma K, Ikeda H, Watanabe K, et al.** (2008) Minimization of exogenous signals in ES cell culture induces rostral hypothalamic differentiation. Proc Natl Acad Sci U S A 105: 11796–11801.

24. **Colleoni S, Galli C, Giannelli SG, Armentero MT, Blandini F, et al.** (2010) Long-term culture and differentiation of CNS precursors derived from anterior human neural rosettes following exposure to ventralizing factors. Exp Cell Res 316: 1148–1158.

25. **James MJ, Jarvinen E, Wang XP, Thesleff I** (2006) Different roles of Runx2 during early neural crest-derived bone and tooth development. J Bone Miner Res 21: 1034–1044.

26. **Lee G, Chambers SM, Tomishima MJ, Studer L** (2010) Derivation of neural crest cells from human pluripotent stem cells. Nat Protoc 5: 688–701.

27. **Ohta S, Imaizumi Y, Okada Y, Akamatsu W, Kuwahara R, et al.** (2011) Generation of human melanocytes from induced pluripotent stem cells. PLoS One 6: e16182.

28. **Fang D, Leishear K, Nguyen TK, Finko R, Cai K, et al.** (2006) Defining the conditions for the generation of melanocytes from human embryonic stem cells. Stem Cells 24: 1668–1677.

29. **Ju C, Zhang K, Wu X** (2012) Derivation of corneal endothelial cell-like cells from rat neural crest cells in vitro. PLoS One 7: e42378.

30. **Umeda K, Zhao J, Simmons P, Stanley E, Elefanty A, et al.** (2012) Human chondrogenic paraxial mesoderm, directed specification and prospective isolation from pluripotent stem cells. Sci Rep 2: 455.

31. **Okamoto T, Aoyama T, Nakayama T, Nakamata T, Hosaka T, et al.** (2002) Clonal heterogeneity in differentiation potential of immortalized human mesenchymal stem cells. Biochem Biophys Res Commun 295: 354–361.

32. **Kreitzer FR, Salomonis N, Sheehan A, Huang M, Park JS, et al.** (2013) A robust method to derive functional neural crest cells from human pluripotent stem cells. Am J Stem Cells 2: 119–131.

33. **Lee G, Ramirez CN, Kim H, Zeltner N, Liu B, et al.** (2012) Large-scale screening using familial dysautonomia induced pluripotent stem cells identifies compounds that rescue IKBKAP expression. Nat Biotechnol 30: 1244–1248.

34. **Kimura C, Takeda N, Suzuki M, Oshimura M, Aizawa S, et al.** (1997) Cis-acting elements conserved between mouse and pufferfish Otx2 genes govern the expression in mesencephalic neural crest cells. Development 124: 3929–3941.

35. **Qiu M, Bulfone A, Ghattas I, Meneses JJ, Christensen L, et al.** (1997) Role of the Dlx homeobox genes in proximodistal patterning of the branchial arches: mutations of Dlx-1, Dlx-2, and Dlx-1 and -2 alter morphogenesis of proximal skeletal and soft tissue structures derived from the first and second arches. Dev Biol 185: 165–184.

36. **Manley NR, Capecchi MR** (1995) The role of Hoxa-3 in mouse thymus and thyroid development. Development 121: 1989–2003.

37. **Liu Z, Yu S, Manley NR** (2007) Gcm2 is required for the differentiation and survival of parathyroid precursor cells in the parathyroid/thymus primordia. Dev Biol 305: 333–346.

38. **Motohashi T, Aoki H, Yoshimura N, Kunisada T** (2006) Induction of melanocytes from embryonic stem cells and their therapeutic potential. Pigment Cell Res 19: 284–289.

39. **Johnston MC, Noden DM, Hazelton RD, Coulombre JL, Coulombre AJ** (1979) Origins of avian ocular and periocular tissues. Exp Eye Res 29: 27–43.

40. **Trainor PA, Tam PP** (1995) Cranial paraxial mesoderm and neural crest cells of the mouse embryo: co-distribution in the craniofacial mesenchyme but distinct segregation in branchial arches. Development 121: 2569–2582.

41. **Fitch JM, Birk DE, Linsenmayer C, Linsenmayer TF** (1990) The spatial organization of Descemet's membrane-associated type IV collagen in the avian cornea. J Cell Biol 110: 1457–1468.

42. **De Schauwer C, Meyer E, Van de Walle GR, Van Soom A** (2011) Markers of stemness in equine mesenchymal stem cells: a plea for uniformity. Theriogenology 75: 1431–1443.

43. **Lee G, Kim H, Elkabetz Y, Al Shamy G, Panagiotakos G, et al.** (2007) Isolation and directed differentiation of neural crest stem cells derived from human embryonic stem cells. Nat Biotechnol 25: 1468–1475.

44. **Curchoe CL, Maurer J, McKeown SJ, Cattarossi G, Cimadamore F, et al.** (2010) Early acquisition of neural crest competence during hESCs neuralization. PLoS One 5: e13890.

45. **Bajpai R, Chen DA, Rada-Iglesias A, Zhang J, Xiong Y, et al.** (2010) CHD7 cooperates with PBAF to control multipotent neural crest formation. Nature 463: 958–962.

46. **Lee G, Papapetrou EP, Kim H, Chambers SM, Tomishima MJ, et al.** (2009) Modelling pathogenesis and treatment of familial dysautonomia using patient-specific iPSCs. Nature 461: 402–406.

47. **Jiang M, Stanke J, Lahti JM** (2011) The connections between neural crest development and neuroblastoma. Curr Top Dev Biol 94: 77–127.

48. **Caplan AI** (2007) Adult mesenchymal stem cells for tissue engineering versus regenerative medicine. J Cell Physiol 213: 341–347.

49. **Silva NA, Sousa N, Reis RL, Salgado AJ** (2013) From basics to clinical: A comprehensive review on spinal cord injury. Prog Neurobiol.

50. **Helms JA, Schneider RA** (2003) Cranial skeletal biology. Nature 423: 326–331.

51. **Morikawa S, Mabuchi Y, Niibe K, Suzuki S, Nagoshi N, et al.** (2009) Development of mesenchymal stem cells partially originate from the neural crest. Biochem Biophys Res Commun 379: 1114–1119.

52. **Takashima Y, Era T, Nakao K, Kondo S, Kasuga M, et al.** (2007) Neuroepithelial cells supply an initial transient wave of MSC differentiation. Cell 129: 1377–1388.

53. **Cai J, Yang M, Poremsky E, Kidd S, Schneider JS, et al.** (2010) Dopaminergic neurons derived from human induced pluripotent stem cells survive and integrate into 6-OHDA-lesioned rats. Stem Cells Dev 19: 1017-1023.

OPEN ACCESS Freely available online

PLOS ONE

Efficient and Rapid Induction of Human iPSCs/ESCs into Nephrogenic Intermediate Mesoderm Using Small Molecule-Based Differentiation Methods

Toshikazu Araoka[1], Shin-ichi Mae[1], Yuko Kurose[1], Motonari Uesugi[2,3], Akira Ohta[1], Shinya Yamanaka[1,4], Kenji Osafune[1]*

1 Center for iPS Cell Research and Application (CiRA), Kyoto University, Kyoto, Japan, **2** Institute for Integrated Cell–Material Sciences, Kyoto University, Kyoto, Japan, **3** Institute for Chemical Research, Kyoto University, Kyoto, Japan, **4** Gladstone Institute of Cardiovascular Disease, San Francisco, California, United States of America

Abstract

The first step in developing regenerative medicine approaches to treat renal diseases using pluripotent stem cells must be the generation of intermediate mesoderm (IM), an embryonic germ layer that gives rise to kidneys. In order to achieve this goal, establishing an efficient, stable and low-cost method for differentiating IM cells using small molecules is required. In this study, we identified two retinoids, AM580 and TTNPB, as potent IM inducers by high-throughput chemical screening, and established rapid (five days) and efficient (80% induction rate) IM differentiation from human iPSCs using only two small molecules: a Wnt pathway activator, CHIR99021, combined with either AM580 or TTNPB. The resulting human IM cells showed the ability to differentiate into multiple cell types that constitute adult kidneys, and to form renal tubule-like structures. These small molecule differentiation methods can bypass the mesendoderm step, directly inducing IM cells by activating Wnt, retinoic acid (RA), and bone morphogenetic protein (BMP) pathways. Such methods are powerful tools for studying kidney development and may potentially provide cell sources to generate renal lineage cells for regenerative therapy.

Citation: Araoka T, Mae S-i, Kurose Y, Uesugi M, Ohta A, et al. (2014) Efficient and Rapid Induction of Human iPSCs/ESCs into Nephrogenic Intermediate Mesoderm Using Small Molecule-Based Differentiation Methods. PLoS ONE 9(1): e84881. doi:10.1371/journal.pone.0084881

Editor: Tadayuki Akagi, Kanazawa University, Japan

Received October 3, 2013; **Accepted** November 20, 2013; **Published** January 15, 2014

Funding: This study was supported in part by research grants from the Leading Project of MEXT, the Uehara Memorial Foundation and the Takeda Science Foundation, by the Japan Society for the Promotion of Science (JSPS) through its "Funding Program for World-Leading Innovative R&D on Science and Technology (FIRST Program)" and Grant-in-Aid for Young Scientists (B) to KO, and by Japan Science and Technology Agency (JST) through PRESTO to KO, JST Yamanaka iPS Cell Special Project to AO, SY and KO, and its research grant "Projects for Technological Development, Research Center Network for Realization of Regenerative Medicine". SM was supported by a fellowship from JSPS. The funders had no role in study design, data collection and analysis, decision to publish, or preparation of the manuscript.

Competing Interests: The authors have declared that no competing interests exist.

* E-mail: osafu@cira.kyoto-u.ac.jp

Introduction

Chronic kidney disease (CKD) is increasingly recognized as a global public health problem. Increased prevalence of CKD has led to a rise in the number of dialysis patients, and is associated with elevated morbidity and mortality due to the increased risk of cardiovascular diseases [1–3]. Most patients with CKD never recover their renal function, and there is a worldwide shortage of donor kidneys for transplantation; therefore, it is important to develop kidney regeneration therapy using embryonic stem cells (ESCs) [4–6] or induced pluripotent stem cells (iPSCs) [7–9], which have unlimited self-renewal capabilities and the potential to differentiate into any cell type in the body. However, directed differentiation methods from human ESCs (hESCs) or iPSCs (hiPSCs) into kidney lineage cells have not been fully developed.

Kidneys are derived from an early embryonic germ layer, the intermediate mesoderm (IM). In vertebrates, the IM sequentially develops into three stages of kidneys; the pronephros, mesonephros and metanephros. The mammalian adult kidney (metanephros) is formed by a reciprocal interaction between two precursor tissues, the metanephric mesenchyme and the ureteric bud [10–13]. Kidney regeneration methods that mimic normal development would first differentiate ESCs or iPSCs into IM, followed by formation of renal progenitors, such as the metanephric mesenchyme and ureteric bud, and eventually produce the various types of fully differentiated renal cells.

Previous research on kidney development in a mouse model showed that expression of a transcriptional regulator, *Odd-skipped related 1* (*Osr1*), starts early in the embryonic day (E) 7.5 IM from which the renal structures are derived [14], and is maintained until kidney organogenesis occurs. *Osr1* knockout mice lack renal structures, due to the failure to form the IM [15,16]. Therefore, differentiation of pluripotent stem cells (PSCs) into *Osr1*-expressing IM cells is the first and crucial step toward the induction of renal lineage cells.

We recently established a highly efficient method for inducing the differentiation of IM cells from human iPSCs/ESCs (hiPSCs/ESCs), in which the combination of activin A and CHIR99021, a glycogen synthase kinase 3β inhibitor, is first used to generate mesendoderm [17,18], followed by combined treatment with bone morphogenetic protein (BMP)-7 and CHIR99021 [19]. This protocol induces development of hiPSCs into $OSR1^+$ IM cells at rate higher than 90%. The $OSR1^+$ IM cells can further differentiate into multiple cell types constituting IM-derived

organs, such as the kidneys, adrenal cortex, and genitalia, both *in vitro* and *in vivo* [19]. Although this method efficiently generates IM cells, modifications are needed for clinical application in kidney regeneration therapy. Growth factors, such as activin A and BMP-7, are expensive, and their effects are inconsistent among different lots. Differentiation methods using low-molecular-weight compounds would be less expensive and more consistent. Small molecules can control cellular processes by modulating signal transduction pathways, gene expression, or metabolism. High-throughput screening has been previously used to identify novel small molecules that support the directed differentiation of mouse ESCs (mESCs) and hESCs into definitive endoderm [20], pancreatic progenitors [21], and cardiomyocytes [22].

In vitro differentiation of the undifferentiated cell mass in the fertilized eggs of amphibians such as Xenopus *laevis* [23–25], mESCs [26–29] and hESCs/iPSCs [30,31] into renal lineages has been stimulated using retinoic acid (RA). However, the roles and mechanisms of RA signaling have remained unclear. Previous studies reported that the signaling pathways of BMP-2 or BMP-4 were involved in the regulation of mesoderm formation, including differentiation of the IM in chick embryos [32,33], but little is known about the developmental mechanisms of IM formation, especially in mammals.

In the present study, we aimed to develop an efficient, stable and low-cost method for differentiating hiPSCs/ESCs into IM cells using small molecules. We performed high-throughput screening of approximately 1,800 chemical compounds and identified two retinoic acid receptor (RAR) agonists, AM580 and TTNPB, that efficiently induce the differentiation of hiPSCs/ESCs into IM cells. Based on these results, we established a simple, rapid, and highly efficient differentiation method, using a combination of just two chemicals (CHIR99021 with TTNPB or AM580), to induce development of hiPSCs/ESCs into IM cells that have the potential to give rise to IM derivatives. We found that combined treatment with CHIR99021 and TTNPB or AM580 induces the differentiation of IM cells by activating the expression of BMP-4 through RAR. We further demonstrated that IM cells can be directly generated from hiPSCs/ESCs without the mesendoderm step, by activating the Wnt, RA, and BMP signaling pathways. The new differentiation method using small molecules provides less expensive and more consistent means of generating IM cells than the growth factor method. Therefore, this new method is useful for studying the mechanisms of mesoderm and kidney development and may provide a source of renal lineage cells for use in regenerative medicine to treat CKD.

Materials and Methods

Cell Culture

Five hiPSC lines (201B6, 253G1, 253G4, 585A1 and an OSR1-green fluorescent protein (GFP) knock-in hiPSC line, 3D45, generated from 201B7 [7,19,34,35]), and three hESC lines (H9, khES1 and khES3 [6,36]), were routinely cultured on feeder layers of mitomycin C-treated mouse SNL feeder cells [37] in Primate ES medium (ReproCELL) supplemented with 500 U/ml penicillin/streptomycin (Invitrogen) and 4 ng/ml recombinant human basic fibroblast growth factor (bFGF, Wako). Cells were split at a ratio of 1:3–1:6 every six to eight days using CTK dissociation solution consisting of 0.25% trypsin (Invitrogen), 0.1% collagenase IV (Invitrogen), 20% Knockout serum replacement (KSR, Invitrogen) and 1 mM $CaCl_2$ in PBS [7].

Chemicals Libraries

The library included compounds from the Prestwick Chemical library (Prestwick Chemical, Illkirch, France) and the ENZO library (ENZO Life Sciences, Farmingdale, NY, USA).

High-throughput Chemical Screening

An OSR1-GFP knock-in hiPSC line, 3D45 [19], grown on mouse embryonic fibroblast (MEF) feeder cells from E 12.5 ICR mouse embryos, were dissociated by an enzymatic method with CTK dissociation solution. After washing them with PBS (Nakalai Tesque), the cells were scraped off with a cell scraper, dissociated by pipetting and seeded on Human Collagen Type I-coated 96-well plates (BD) with MEF-conditioned Primate ES medium containing 10 ng/ml bFGF. When hiPSC colonies attained approximately 70% confluency, the cells were treated with 100 ng/ml recombinant human/mouse/rat activin A (R&D Systems), 3M CHIR99021 (Wako) and 10 μM Y27632 (Wako) in Stage 1 medium containing DMEM/F12+Glutamax (Invitrogen) supplemented with 500 U/ml penicillin/streptomycin, 2% FBS (HyClone) and 10 μM Y27632 for two days. Then, the compound treatments were performed at a final concentration of 1 μM in 100 μl of Stage 2 medium containing DMEM/F12+Glutamax supplemented with 0.1 mM non-essential amino acids (Invitrogen), 500 U/ml penicillin/streptomycin, 0.55 mM 2-mercaptoethanol (Invitrogen) and 10% KSR supplemented with 0.1% DMSO (v/v) per well. After five days of compound treatments, the cells were dissociated by trypsinization, resuspended in HBSS with propidium iodide (1:1000, Wako) and examined for their GFP expression by a LSR Fortessa equipped with a High Throughput Sampler (BD). Positive hits were defined as the compounds that induced GFP^+ cells at three standard deviations (3SD) above the DMSO controls without producing autofluorescence or cytotoxicity.

Generation of Efficacy Curves

The OSR1-GFP knock-in hiPSCs (3D45) were dissociated and plated onto Matrigel-coated 96-well plates in Stage 1 medium with 100 ng/ml activin A, 3 μM CHIR99021 and 10 μM Y27632. After two days of Stage 1 treatment, AM580 or TTNPB was added at a final concentration of 10 μM, 5 μM, 2.5 μM, 1.2 μM, 600 nM, 300 nM, 150 nM, 75 nM, 37.5 nM, 19 nM, 10 nM, 5 nM, 2.5 nM, 1.2 nM, 0.6 nM or 0.3 nM. Five days later, the induction of $OSR1^+$ cells was detected by flow cytometry. For the replacement of TTNPB or AM580 in the small molecule method, all-trans retinoic acid (ATRA), adapalene, or CD1530 was added at a final concentration of 10 μM, 5 μM, 2.5 μM, 1.2 μM, 600 nM, 300 nM, 150 nM, 75 nM, 37.5 nM, 19 nM, 10 nM, 5 nM or 2.5 nM, and BMS493, LE135, MM11253 or SR11237 was used at a final concentration of 10 μM, 5 μM, 2.5 μM, 1.0 μM, 100 nM, 10 nM, 1.0 nM or 0.1 nM. The induction of $OSR1^+$ cells was analyzed by flow cytometry on day 6 of treatment. For the addition of SR11237 or UVI3003 to the TTNPB method, these chemicals were added at final concentrations of 5 μM, 2.5 μM, 1.0 μM, 100 nM, 10 nM or 1.0 nM. The details of the growth factors and chemical compounds used in this study are shown in Table S4.

Differentiation Methods

To induce IM cells, hiPSC/ESC colonies grown on feeder layers of mitomycin C-treated mouse SNL feeder cells [37] were first dissociated by an enzymatic method with CTK dissociation solution, and incubated on gelatin-coated plates for 30 min to remove SNLs. Then, the cells were dissociated into single cells by

gentle pipetting after the treatment with Accutase (Innovative Cell Technologies, Inc.) for 20 min. The cells were then seeded on Matrigel (Matrigel Matrix Growth Factor Reduced, BD)-coated plates at a density of 1.5×10^5 cells/cm^2.

For the original small molecule methods, the dissociated hiPSCs/ESCs were treated with 3 μM CHIR99021 and 1 μM AM580 (Santa Cruz Biotechnology) or 1 μM TTNPB (Santa Cruz Biotechnology) in Stage 1 medium for two days. Next, the culture medium was replaced with Stage 2 medium containing 1 μM AM580 or 1 μM TTNPB. The Stage 2 cultures were maintained for an additional three to 12 days. The growth factor method was previously described as a "single-cell method" [19].

For the serum-free small molecule methods, the cells were cultured with a serum-free medium containing DMEM/F12 + Glutamax supplemented with 1×B27 supplement (Invitrogen) and 500 U/ml penicillin/streptomycin on Synthemax (Synthemax II-SC Substrate, Corning)-coated plates throughout the differentiation culture.

Flow Cytometry and Cell Sorting

The cells were treated with 0.25% trypsin/EDTA for 5 min at 37°C, and dissociated by pipetting in HBSS (GIBCO). Dead cells stained with propidium iodide were excluded from the analysis. The cells were analyzed and sorted using a FACS Aria II cell sorter (BD). The isolated cells were collected in PBS with 2% FBS containing 10 μM Y27632.

RT-PCR and Real-time Quantitative RT-PCR (qRT-PCR)

Total RNA was isolated from triplicate samples in three independent experiments using an RNeasy kit (Qiagen) according to the manufacturer's recommendations, followed by cDNA synthesis using standard protocols. Briefly, first-strand cDNA was synthesized from 1 μg of total RNA using ReverTra Ace (TOYOBO). The cDNA samples were subjected to PCR amplification using a thermal cycler (Veriti 96 well Thermal Cycler, Applied Biosystems). PCR was performed using the Ex-Taq PCR kit (Takara) according to the manufacturer's instructions. The PCR cycles were as follows: for *β-ACTIN*, initial denaturation was performed at 94°C for 2.5 min, followed by 25 cycles of 94°C for 30 s, 60°C for 1 min, 72°C for 30 s, and a final extension at 72°C for 10 min. For the other genes, the cycles consisted of initial denaturation at 94°C for 2.5 min, followed by 30–40 cycles of 94°C for 30 s, 58–62°C for 30 s, 72°C for 30 s, and final extension at 72°C for 7 min. mRNA from human fetal kidney was used as a positive control for expression of *OSR1*, *PAX2*, *LIM1*, *WT1*, *EYA1*, *SALL1*, and *CITED2*. mRNA from human adult ovaries was used as a positive control for *SOX17*. mRNA from neural progenitor cells, induced from hiPSCs by SFEBq culture [38], was used as a positive control for *SOX1*. mRNA from human umbilical vein endothelial cells (HUVECs) was used as a positive control for *KDR*. mRNA from human adult cervix was used as a positive control for *SIX2*. mRNA from human adult kidney was used as a positive control for *HOXD11*, *FOXD1*, *SALL4*, and *HOXB7*. mRNA from human adult ovaries was used as a positive control for *GATA4* and *GATA6*. mRNA from human adult adrenal gland was used as a positive control for *SF1* and *HSD3β2*. mRNA from human adult testes was used as a positive control for *DAX1* and *LHX9*. qPCR was performed using the Step One Plus Real-Time PCR System (Applied Biosystems) and the SYBR Green PCR Master Mix (Takara). Denaturation was performed at 95°C for 30 s, followed by 45 cycles at 95°C for 5 s and at 60°C for 30 s. The threshold cycle method was used to analyze the data for the gene expression levels as recommended by the manufacturer, and was calibrated to the levels of the housekeeping gene, *β-ACTIN*. The PCR reactions were performed in triplicate for each sample. The primer sets are shown in Table S2.

Immunostaining

The cells were fixed with 4% paraformaldehyde (PFA, Nacalai Tesque)/PBS for 20 min at 4°C. For immunostaining of the cytoplasm, the cells were washed with PBS and blocked with 5% normal donkey serum (Chemicon)/PBST (PBS/0.1% Triton X-100, Nacalai Tesque) for 1 hr at room temperature. The primary antibodies were diluted in blocking solutions and incubated with samples overnight at 4°C. For nuclear immunostaining, the cells were washed with PBS and incubated in PBS/0.2% Tween 20 (Wako) for 30 min at room temperature, followed by blocking with 3% normal donkey serum/1% BSA (Nacalai Tesque)/PBST (PBS/0.25% Triton X-100) for 1 hr at room temperature. The primary antibodies were diluted in blocking solution and incubated with samples overnight at 4°C. Secondary antibodies were diluted in blocking solution and incubated with samples for 1 hr at room temperature. The details of the antibodies used in this study are shown in Table S3.

In Vitro Differentiation Culture of OSR1$^+$ Cells

The OSR1$^+$ IM cells induced with the TTNPB method were isolated by flow cytometry sorting on culture day 6, seeded onto gelatin-coated 96-well plates at a density of 1.0×10^5 cells/well, and cultured with Stage 2 medium containing 10 μM Y27632, 100 ng/ml recombinant human BMP-7 and 100 ng/ml recombinant mouse Wnt3a or 1 μM CHIR99021 [19]. After an additional eight days of culture, the cells were examined by RT-PCR and immunostaining.

Graft Preparation and Implantation

The hiPSC-derived OSR1$^+$ on culture day 6 was isolated by flow cytometry sorting, seeded onto low attachment 96-well plates (Lipidure Coat, NOF Corp) at a density of 1.0×10^5 cells per well, and cultured with Stage 2 medium containing 10 μM Y27632 for 2 days. Then, about 20 aggregates were transferred onto polyethylene terephthalate fiber-Collagen Sponge (MedGEL) that was prewetted with Stage 2 medium. The aggregates and sponge were overlayed with 50 l of Matrigel. The resultant implant constructs were placed in an incubator set at 37°C and 5% CO_2 for 1 h to allow the construct to gel. These constructs were transferred to culture dishes with prewarmed medium until implantation. One of the epididymal fat pads (EFPs) of immunodeficient mice (NOD. CB17-*Prkd*^{scid}/J) was carefully externalized through an abdominal incision, then a single implant construct was wrapped in the EFP and the implanted EFP were returned to abdominal cavity. After 4 weeks of implantation, mice were killed and the serial sections of implanted tissues were examined with immunostaining [19].

Aggregate Culture of OSR1$^+$ Cells

The day 6 isolated OSR1$^+$ IM cells differentiated with the TTNPB method were quickly seeded onto 96-well low-cell-adhesion plates (Lipidure Coat, NOF Corp) with Stage 2 medium (1.0×10^5 cells in 100 l/well) containing 10 M Y27632, and then were cultured at 37°C to form cellular aggregates. After eight days of suspension culture, the aggregates were fixed, and serial sections were examined by immunostaining. Stained sections were analyzed with a LSN710 confocal microscope (Zeiss).

Organ Culture Experiments

The organ culture experiments were performed as described previously [19,39]. Briefly, E 11.5 metanephric kidneys from ICR mice were dissected in Improved MEM (Invitrogen). The metanephric kidneys were then placed in 0.05% trypsin-EDTA (GIBCO) for 10 min at 37°C and dissociated by pipetting. The dissociated cells were stabilized in Improved MEM supplemented with 500 U/ml penicillin/streptomycin and 10% FBS (Kidney culture medium, KCM) for 10 min at 37°C, and then were filtered through a 40 m cell strainer (BD). A total of 1.0×10^5 freshly dissociated metanephric cells and 1.0×10^4 $OSR1^+$ cells isolated by flow cytometry sorting after the induction with the small molecule methods were mixed, seeded onto 96-well low-cell-adhesion plates with 10 M Y27632, then cultured overnight at 37°C to form aggregates. The cellular aggregates were then cultured at the air-fluid interface on 0.4 m pore polycarbonate filters (Millipore) supplied with KCM at 37°C. After eight days of organ culture, the aggregates were fixed, and serial sections were examined by immunostaining.

Statistical analysis

The statistical significance of the differences in the frequency of renal tubule formation between the hiPSC-derived $OSR1^+$ cells generated with small molecule treatments and the control undifferentiated hiPSCs in organ culture was analyzed using Fisher's exact test.

Animal Welfare

This study was carried out in strict accordance with the recommendations in the Regulation on Animal Experimentation at Kyoto University. The protocol in this study was approved by the Animal Research Committee of Kyoto University. All efforts were made to minimize suffering. Mice were humanely sacrificed prior to tissue collection.

Inhibitor Screening

The effects of 18 different chemical inhibitors on the induction of $OSR1^+$ IM cells with the TTNPB method were examined at different concentrations, as indicated in Figure S4. After 72 hrs of treatment, the cells were examined by the same procedures used for the high-throughput chemical screening described above. The details of the growth factors and chemical compounds used in this study are shown in Table S4.

Western Blot Analysis

The cells treated with the small molecule methods were harvested in lysis buffer (BioVision). Proteins were separated by 10% Tris-Glycine SDS/PAGE (BIO-RAD) under denaturing conditions and transferred to a PVDF membrane (BIO-RAD). After blocking with 5% skim milk in PBS/0.1% Tween20, the membrane was incubated with antibodies against phospho-Smad1/5 or β-actin overnight at 4°C. The membrane was then washed, incubated with anti-mouse/rabbit peroxidase-conjugated secondary antibody (Jackson ImmunoResearch) at room temperature for 1 hr and developed by a chemiluminescence detection system (GE Healthcare).

Gene Knockdown Experiments

The dissociated OSR1-GFP knock-in hiPSCs (3.0×10^4 cells in 0.5 ml/well of 24-well plates) in Stage 1 medium with 3 M CHIR99021, 1 M TTNPB, and 10 M Y27632 were transfected with 50 nM siRNA for *RARB* (MISSION siRNA, Sigma) or Universal Negative Control siRNA Duplex (Stealth RNAi Negative Control Kit, Invitrogen) using the Lipofectamine RNAiMAX reagent (Invitrogen) throughout Stage 1. After 48 hrs of Stage 1 treatment, the cells were transfected again, this time with Stage 2 medium containing 1 M TTNPB and the same siRNA solutions used in Stage 1.

Results

High-throughput Screening Identified Small Molecules that Induce Production of IM Cells from hiPSCs

The screen used an hiPSC reporter line, in which the GFP coding sequence had been knocked-in to the OSR1 gene locus (OSR1-GFP knock-in hiPSC line, 3D45; [19]) and flow cytometry to quantitatively identify small molecules that increase the induction rate of $OSR1^+$ cells. Mesendoderm cells, the starting material for the screen, were generated from hiPSCs (3D45 cells) using a combination of 100 ng/ml activin A and 3 μM CHIR99021 for two days (Figure 1A, Stage 1), as described previously [19]. The mesendoderm cells were then treated with individual compounds for an additional five days (Stage 2). We screened two chemical libraries, the Prestwick Chemical library and ENZO library, comprising a total of 1,821 bioactive compounds and known drugs. Positive hits were defined as compounds that induced OSR1 $(GFP)^+$ cells at three standard deviations (3SD) above the negative control (DMSO), without producing autofluorescence or cytotoxicity. The $OSR1^+$ IM cells induced by the combination of CHIR99021 and BMP-7, which we described previously [19], were used as a positive control.

The screening identified two compounds, AM580 and TTNPB, both known to be RAR agonists, as inducers of $OSR1^+$ cells (Figure 1B). The induction rates of $OSR1^+$ cells in populations treated with AM580 (64.3±7.4%, n = 3) or TTNPB (53.6±21.5%, n = 3) were higher than rates for DMSO-treated controls (1.6±0.4%, n = 3) and positive controls (47.9±0.8%, n = 3) (Figure 1C).

Additional experiments were carried out to optimize the concentrations of the compounds. Titration curves from 0.3 nM to 1.2 M for AM580 and TTNPB showed that both compounds induced $OSR1^+$ cells in a dose-dependent manner, with the highest efficiencies at 300 nM to 1.2 M for AM580, and at 37.5 nM to 1.2 M for TTNPB (Figure 1D).

A Small Molecule-based Differentiation Method Rapidly and Efficiently Produces IM Cells from hiPSCs

Previous studies reported that the activation of Wnt signaling by recombinant Wnt proteins or chemicals resulted in the differentiation of mESCs and hESCs into mesendoderm without activin A treatment [40,41]. Results of the present study confirmed that mesendoderm cells were induced from hiPSCs by the treatment with CHIR99021 alone (Figures S1A and B). To further optimize the method for generating $OSR1^+$ cells, we examined various combinations of CHIR99021 with AM580 or TTNPB, without activin A (Figure 2A). We found that, when hiPSCs were treated with 3 M CHIR99021 combined with 1 M AM580 or 1 M TTNPB for two days during Stage 1, and with 1 M AM580 or 1 M TTNPB for an additional three days during Stage 2, the induction rate of $OSR1^+$ cells on day 6 was increased to around 80% (Small molecule method, including AM580 and TTNPB methods, Figure 2B and Figure S2A). The numbers of $OSR1^+$ and total cells peaked on culture day 11 (Figure 2C and Figure S2B). The small molecule method induced a much larger number of $OSR1^+$ cells than our growth factor method [19] at all of the tested time points. Therefore, we established a rapid (requiring only five days), highly efficient (approximately 80%) and robust

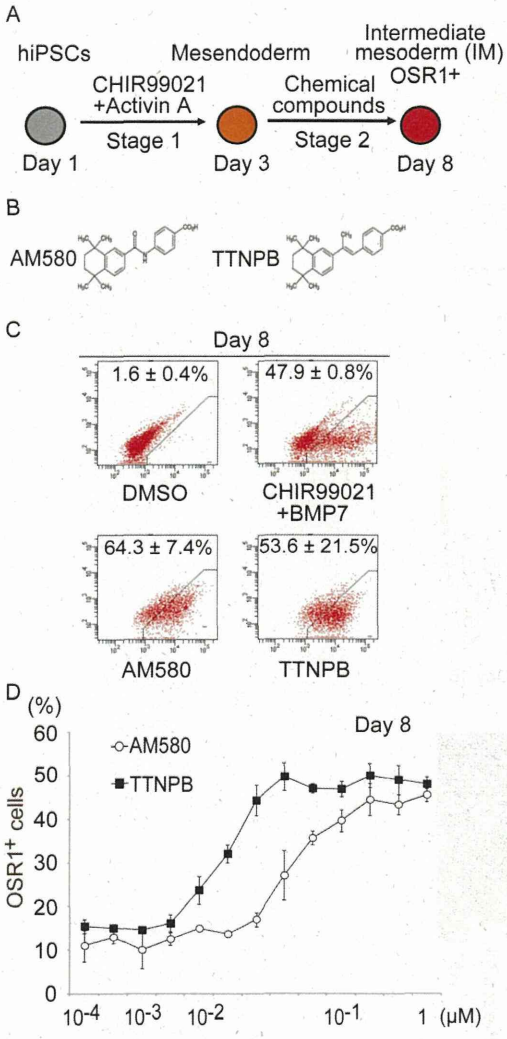

Figure 1. High-throughput Screening and Characterization of the Two Hit Compounds. (A) Schematic diagram of the screening strategy to induce the differentiation of human iPSCs (hiPSCs) into intermediate mesoderm (IM). Stage 1 indicates the differentiation step from hiPSCs into mesendoderm. Stage 2 indicates differentiation from mesendoderm into IM. Chemical screening was performed on Stage 2 cells. (B) The chemical structures of the two hit compounds, AM580 and TTNPB. (C) Results of flow cytometric analyses of the induction of OSR1$^+$ cells on culture day 8; treatments consisted of two days of Stage 1 with CHIR99021 and activin A, and five days of Stage 2 with AM580 or TTNPB, DMSO (negative control), or combined CHIR99021 and BMP7 (positive control). (D) Dose-response curve of OSR1$^+$ cell induction on day 8 by AM580 and TTNPB. The data in (C) and (D) are means±SD of three independent experiments (n = 3).
doi:10.1371/journal.pone.0084881.g001

differentiation method for generating OSR1$^+$ cells from hiPSCs using only two chemicals.

The development of a well-defined method for differentiating PSCs would provide an excellent system that could be used to elucidate the molecular mechanisms of IM differentiation. We therefore devised a serum-free differentiation method by replacing both fetal bovine serum (FBS) used in Stage 1 and KSR in Stage 2 of the small molecule method with B27 supplement. Moreover, Matrigel which coated dishes was replaced by Synthemax, xeno-free coating material. The induction efficiency of OSR1$^+$ cells in the refined protocol (Serum-free small molecule method, including Serum-free AM580 and TTNPB methods) was about 80% and comparable to the original small molecule method (Figure 2D).

To confirm that the human OSR1$^+$ cells induced by the small molecule method have an IM signature, we used RT-PCR analyses and immunocytochemistry to examine the expression of multiple IM marker genes. After five days of treatment, the OSR1$^+$ cells isolated by flow cytometry sorting expressed *PAX2*, *LIM1*, *WT1*, *EYA1*, *SALL1*, and *CITED2* (Figure 2E), which are all known to be expressed in cells of IM or kidney lineage [12,14]. Moreover, some of the OSR1$^+$ cells isolated on culture day 6 were positively stained for SALL1, WT1, LIM1, or PAX2 (Figure 2F). In contrast, markers for non-IM lineage cells, including *SOX17* for endoderm, *SOX1* for ectoderm, and *KDR* for lateral plate mesoderm, were not detected (Figure 2E). Most of the OSR1$^+$ cells produced by the small molecule method appear to represent the IM.

As it has been demonstrated that different hiPSC/ESC lines vary in their differentiation potential [34,42], we examined effectiveness of the small molecule method using multiple hiPSC/ESC lines (Figure S3) [6,7,34–36]. The results confirmed that the method works with dermal fibroblast-derived iPSC lines (201B6, 253G1, and 253G4), a peripheral blood cell-derived iPSC line (585A1), and hESC lines (KhES1, KhES3, and H9), in addition to the 3D45 cells (201B7).

IM Cells Generated with the Small Molecule Method Can Differentiate into IM Derivatives and Form Renal Tubule-like Structures

Osr1$^+$ IM cells contribute to a variety of cell types during embryonic development in mice, including cells of the adrenal cortex and gonad, as well as kidney [14]. We recently demonstrated that hiPSC-derived OSR1$^+$ IM cells generated by the growth factor method differentiated into these cell types, following an additional seven-day treatment with 100 ng/ml BMP-7 and 100 ng/ml Wnt3a or 1–3 M CHIR99021 [19]. In the present study, we treated OSR1$^+$ cells isolated on culture day 6 of the small molecule method with these factors for an additional eight days to examine their developmental potential to give rise to IM-derivative cell types (Figure 3A, upper panel). The treated cells expressed marker genes for IM-derivative cell types, including *SIX2* and *HOXD11* for the metanephric mesenchyme; *FOXD1* for metanephric stroma; *SALL4* and *HOXB7* for the nephric duct and ureteric bud; and *GATA4*, *GATA6*, *SF1*, *HSD3β2*, *DAX1* and *LHX9* for gonadal or adrenocortical cells (Figure 3B). The differentiated cells also stained positively for a number of renal lineage markers: *Lotus tetragonolobus* lectin (LTL) and aquaporin 1 (AQP1) for the proximal renal tubule, podocalyxin (PDX) and WT1 for glomerular podocytes, *Dolichos biflorus* agglutinin (DBA) and cytokeratin 8 (CK8) for nephric duct and ureteric bud, αSMA for smooth muscle, E-cadherin (ECAD) for epithelia, and GATA6 and HSD3β for the gonad or adrenal cortex (Figure 3C).

Next, to assess the developmental potential of hiPSC-derived IM cells *in vivo*, we transplanted day 6 OSR1$^+$ cells generated with the TTNPB method into the epididymal fat pads (EFPs) of immunodeficient mice (NOD. CB17-*Prkdc*^{scid}/J) (Figure 3A, upper middle panel). At four weeks after transplantation, grafts from five independent experiments contained cells immunoreactive for adult renal cell markers, such as AQP1 and LTL (Figure 3D), with no evidence of either teratomas or the formation of three-dimensional renal structures, which was similar to the findings obtained from the transplantation of hiPSC-derived IM cells generated with the growth factor method, as described previously [19].

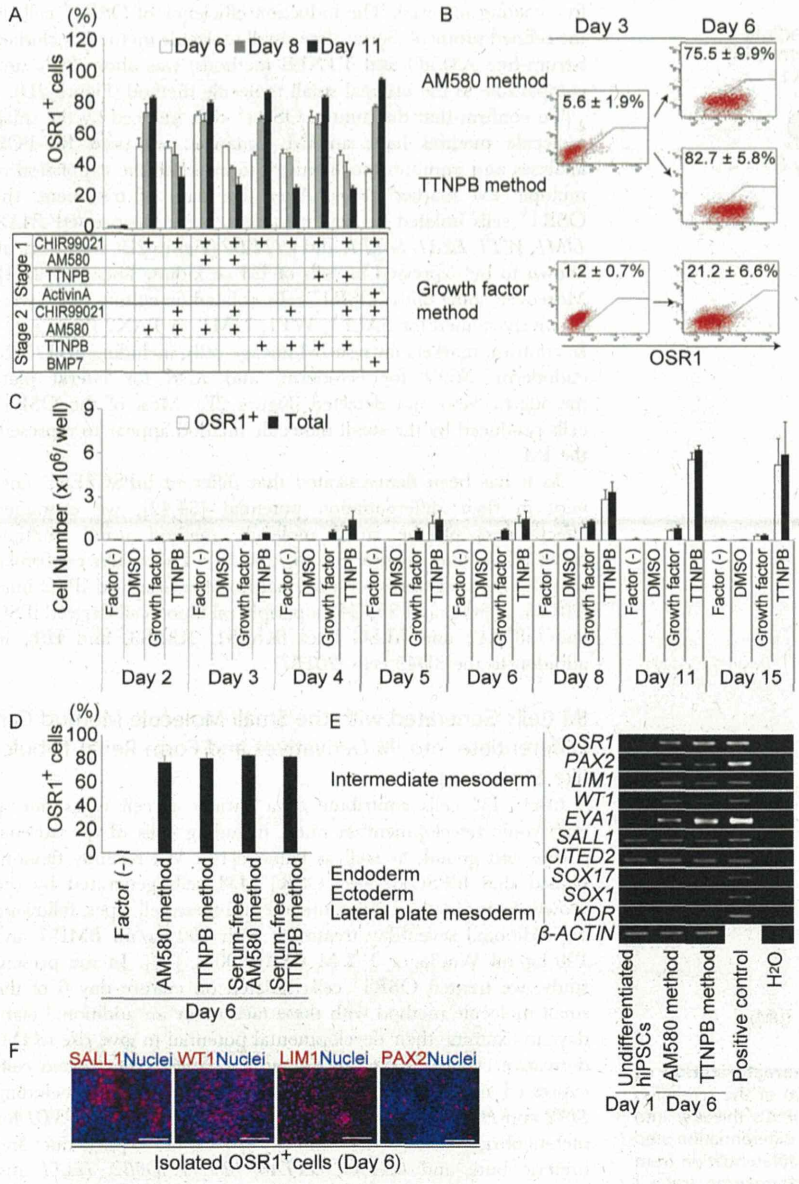

Figure 2. The Small Molecule Method for Differentiating hiPSCs into IM Cells. (A) The results of the flow cytometric analyses comparing the induction efficiency of $OSR1^+$ cells on culture days 6, 8, and 11 for various treatments with CHIR99021 and AM580 or TTNPB, and the growth factor method (CHIR99021 and activin A during Stage 1, CHIR99021 and BMP7 during Stage 2). (B) Results of flow cytometric analyses of $OSR1^+$ cell induction on days 3 and 6 of the AM580, TTNPB, and growth factor methods. (C) Numbers of $OSR1^+$ and total cells generated by the TTNPB and growth factor methods. (D) Results of the flow cytometric analyses showing the differentiation of $OSR1^+$ cells on day 6 using the serum-free small molecules methods. (E) Results of RT-PCR analyses showing mRNA expression of IM and non-IM marker genes in undifferentiated hiPSCs before treatment on day 1, and in $OSR1^+$ cells on day 6 after induction by the small molecule method. (F) Immunostaining for SALL1, WT1, LIM1, and PAX2 in the $OSR1^+$ cells on day 6 of induction by the TTNPB method. Scale bars, 100 m. The data in (A–D) are means±SD of three independent experiments (n = 3). The data in (E) and (F) are representative of three independent experiments. See Figure S2 for additional data.
doi:10.1371/journal.pone.0084881.g002

To further evaluate the multi-lineage differentiation potential, cellular aggregates were generated from the $OSR1^+$ IM cells, by culturing them in non-attachment dishes for an additional eight days with a ROCK inhibitor, Y27632, that increases the survival rate of dissociated hiPSCs/ESCs and the cells differentiated from them [34,43] (Figure 3A, lower middle panel). The aggregates contained cells that were positively immunostained for IM-derivative markers, including SALL4 for the nephric duct and ureteric bud, AQP2 for the collecting duct, and GATA4 for the gonad and adrenal cortex (Figure 3E). Furthermore, renal tubule-like structures were formed inside the aggregates, which were positive for ECAD, LTL, and a polarized epithelial marker, laminin (Figure 3F).

The ability of the hiPSC-derived $OSR1^+$ cells produced by the small molecule method to differentiate into three-dimensional renal structures was further examined by co-culturing them with

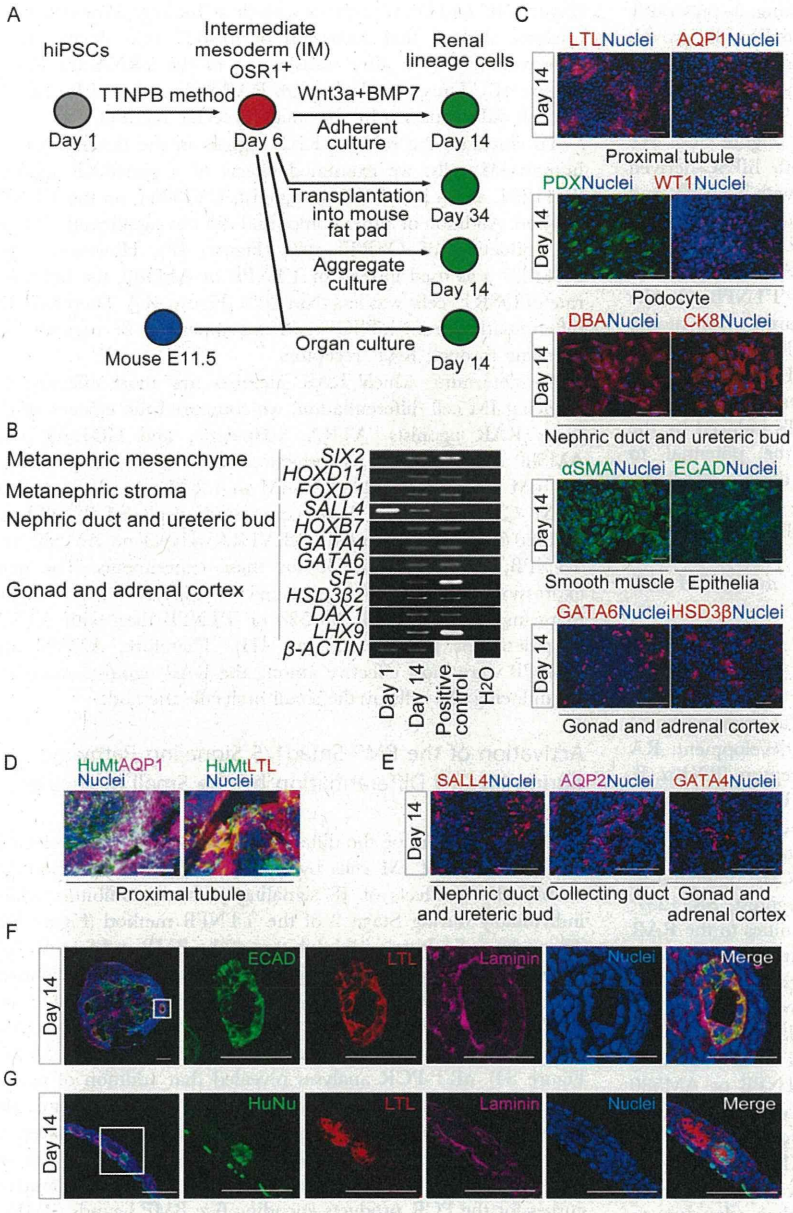

Figure 3. Developmental Potential of hiPSC-derived IM Cells Generated by the Small Molecule Method. (A) Schematic showing further *in vitro* and *in vivo* development of OSR1^{+} cells that were differentiated from OSR1-GFP knock-in hiPSCs (3D45), using the TTNPB method. (B) Results of RT-PCR analyses showing mRNA expression of marker genes for the developing kidney, gonad, and adrenal cortex in differentiated OSR1^{+} cells on culture day 14. (C) Differentiated cells stained on day 14 with antibodies or lectins against markers of IM derivatives: LTL and AQP1 for the proximal renal tubule, PDX and WT1 for glomerular podocytes, DBA and CK8 for the nephric duct and ureteric bud, &SMA for smooth muscle, ECAD as an epithelial marker, and GATA6 and HSD3β as markers of gonad or adrenal cortex. (D) Immunostaining of histological sections of four-week-old hiPSC-derived IM grafts generated by the TTNPB method transplanted into immunodeficient mice (NOD. CB17-*Prkdc*^{scid}/J) for human mitochondria (HuMt) (green), LTL (red), AQP1 (purple) and all nuclei (blue). (E) Immunostaining for IM derivative markers (SALL4 for the nephric duct and ureteric bud, AQP2 for the collecting duct, and GATA4 for the gonads or adrenal cortex) of histological sections of cell aggregates generated from OSR1^{+} cells isolated on day 6 and grown in suspension culture for an additional 8 days. (F) Renal tubule-like structures formed inside the cell aggregates on day 14 stained for ECAD (green), LTL (red), laminin (purple), and nuclei (blue). The five panels on the right are magnified views of the solid box in the left panel. (G) Section immunostaining of organ culture samples collected on day 14, for human nuclei (HuNu, green), LTL (red), laminin (purple), and all nuclei (blue). The five panels on the right are magnified views of the solid box in the left panel. The data in (B, C), (D) and (E, F) are representative of the findings of three, five and four independent experiments, respectively. Scale bars, 100 m.
doi:10.1371/journal.pone.0084881.g003

mouse metanephric cells in an organ culture setting, as previously described using hiPSC-derived IM cells generated by the growth factor method [19,39] (Figure 3A, lower panel). The human $OSR1^+$ cells were integrated into the mouse metanephric tissues and differentiated into polarized tubule-like structures, which stained positively for both LTL and laminin (Figure 3G). We examined 145 organ culture samples: 37 with hiPSC-derived $OSR1^+$ cells induced with AM580, 49 induced with TTNPB, and 59 controls with undifferentiated hiPSCs. Human LTL^+/$laminin^+$ renal tubule-like structures originated from the $OSR1^+$ IM cells in 18 out of the 37 samples (48.6%) induced using AM580, and in 24 out of the 49 samples (49.0%) generated using TTNPB. On the other hand, undifferentiated hiPSCs co-cultured with mouse metanephric cells did not form any kidney-like structures or express any of the markers (0%, $n = 59$; AM580 vs. undifferentiated hiPSCs, $p<0.001$; TTNPB vs. undifferentiated hiPSCs, $p<0.001$). Thus, hiPSC-derived $OSR1^+$ IM cells induced by the small molecule method appear to have the potential to differentiate into IM derivatives and to form three-dimensional renal structures.

These results suggest that the human IM cells generated with the small molecule method have the potential to become renal lineage cells both *in vitro* and *in vivo*, similar to the IM cells generated with the growth factor method [19].

IM Differentiation by the Small Molecule Method Involves RARβ Signaling

Two families of RA nuclear receptors act as transcriptional transducers of retinoid signals during normal development: RA receptors (RARα, β, and γ) and retinoid X receptors (RXRα, β, and γ) [44,45]. To determine which RAR and RXR isotypes are activated during human IM cell differentiation by the small molecule method, we examined the effects of three RAR agonists, ATRA, adapalene, and CD1530; three RAR antagonists, BMS493, LE135, and MM11253; one RXR agonist, SR11237; and one RXR antagonist, UVI3003, whose affinities to the RAR and RXR isotypes are concentration-dependent (Table S1) [46–49]. It has been reported that signals through RAR, but not through RXR, are involved in the mESC differentiation into IM cells [29]. In addition, TTNPB and AM580 are known to be RAR agonists, so we first examined the roles of RAR signaling pathways. Induction of $OSR1^+$ cells when TTNPB or AM580 was replaced with adapalene (a RARβγ agonist) required concentrations greater than 10–75 nM, suggesting that the adapalene works mainly through RARβ or RARγ. Replacement of TTNPB or AM580 with CD1530, a selective RARγ agonist, required about 100 times higher concentration than adapalene to induce $OSR1^+$ cells, indicating that signals through RARγ might not play central roles in IM differentiation (Figure 4A and Table S1). Together, these results suggest that the IM cell differentiation from hiPSCs in the small molecule method is primarily mediated by RARβ signaling.

To further analyze the roles of RAR isotypes, we added RAR antagonists to the TTNPB method: a pan-RAR antagonist, BMS493; a selective RARβ antagonist, LE135; and a selective RARγ antagonist, MM11253 (Figure 4B). Induction of $OSR1^+$ cells was reduced by adding BMS493 or LE135, but not by adding MM111235, confirming the involvement of RARβ signaling in IM cell differentiation.

We also examined the effects of small-interfering RNA (siRNA) targeting RARβ on the induction of IM cells in the TTNPB method. The addition of siRNA for RARβ, which silenced around 70% of *RARβ* expression, reduced *OSR1* gene expression by approximately 70%, compared to cells treated with control siRNA (Figures 4C and D). Consistent with these findings, flow cytometry analyses showed that induction of $OSR1^+$ cells decreased by approximately 40% after transfection of the siRNA for RARβ (Figure 4E). Thus, signals through RARβ are essential for human IM cell differentiation by the small molecule method.

To elucidate the roles of RXR signals in the development of human IM cells, we examined effects of a pan-RXR agonist, SR11237, and a pan-RXR antagonist, UVI3003, on the TTNPB method. Addition of either compound did not significantly change the induction of $OSR1^+$ cells (Figure 4F). However, when SR11237 was used instead of TTNPB or AM580, the induction rate of $OSR1^+$ cells was less than 20% (Figure 4G). Therefore, IM differentiation from hiPSCs does not appear to be regulated by signaling through RXR receptors.

To determine which RAR agonists are most effective for inducing IM cell differentiation, we compared the efficacy of the three RAR agonists (ATRA, adapalene, and CD1530) with AM580 and TTNPB. As induction of $OSR1^+$ cells peaked at 150 nM to 2.5 M ATRA, 150 nM to 1.2 M adapalene, and 5–10 M CD1530, when those compounds replaced TTNPB or AM580 (Figure 4A), we used 1 M ATRA, adapalene, AM580, and TTNPB, and 5 M CD1530 for these experiments. The gene expression level of *OSR1*, analyzed by qRT-PCR, was higher following treatment with AM580 or TTNPB than with ATRA, adapalene, or CD1530 (Figure 4H). Therefore, AM580 and TTNPB were most effective among the RAR agonists examined for inducing IM cells by the small molecule method.

Activation of the BMP-Smad1/5 Signaling Pathways during IM Cell Differentiation by the Small Molecule Method

To further examine the differentiation mechanisms involved in the generation of IM cells by the small molecule method, we examined the effects of 18 signaling pathway inhibitors added individually during Stage 2 of the TTNPB method (Figure S4). Three days of culture with inhibitors of the BMP and Smad1/5/8 signaling pathways, including noggin (a BMP antagonist), dorsomorphin (an ALK2/3/6 inhibitor), LDN193189 (an ALK2/3 inhibitor), and DMH1 (an ALK2 inhibitor), reduced induction of IM cells in a dose-dependent manner (Figure 5A and Figure S4). qRT-PCR analyses revealed that addition of noggin inhibited up-regulation of *OSR1* gene expression (Figure 5B), indicating that BMP signaling pathways might be involved in differentiation of IM cells. To determine which BMP ligands are expressed during the induction process, we generated standard curves for the PCR products encoding five BMP ligands (BMP-2, 4, 5, 6, and 7), and analyzed the copy number of each ligand in cDNA samples of hiPSC-derived $OSR1^+$ cells on day 6. *BMP-4* was the most abundantly expressed, and *BMP-5* showed the second highest expression (Figure 5C). Their expression levels gradually increased in a time-dependent manner until culture day 5. Interestingly, expression of *BMP-4* began to increase during Stage 1, around culture day 2 (Figure 5D), suggesting that the small molecule method with CHIR99021 and TTNPB activates *BMP-4* expression and Smad1/5/8 signaling pathways prior to day 3.

When noggin or DMH1 were added beginning on day 1 of the small molecule method, both $OSR1^+$ cell differentiation and *OSR1* gene expression decreased more than when these factors were added at Stage 2 (Figures 5A, B, E and F). Immunoblot analyses detected high levels of Smad1/5 phosphorylation in cell lysates of hiPSC differentiation culture on day 6 of the small molecule method with CHIR99021 and AM580 or TTNPB. Phosphoryla-

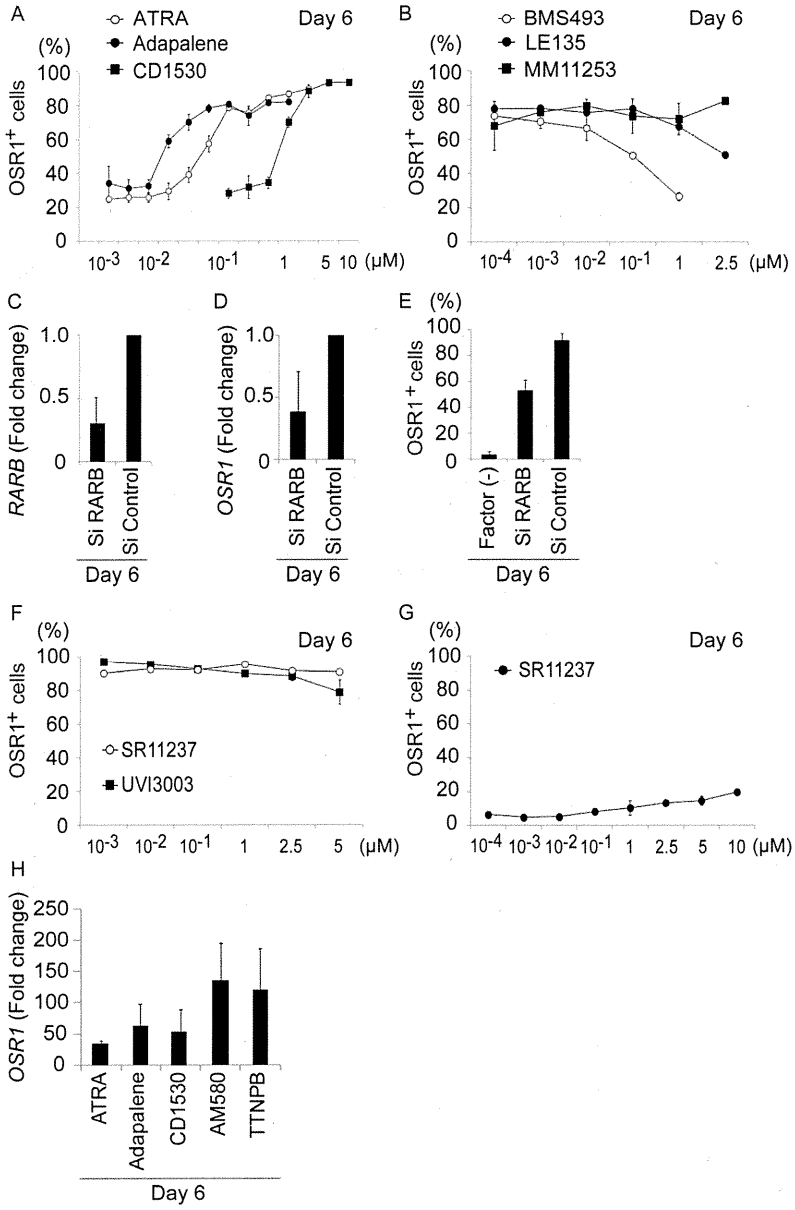

Figure 4. The Small Molecule Method Functions via RARβ Receptors. (A) Results of the flow cytometric analyses showing induction of OSR1$^+$ cells by the small molecule method, when AM580 or TTNPB was replaced by all-trans retinoic acid (ATRA), adapalene, and CD1530. (B) Effects of adding RAR antagonists, BMS493, LE135, and MM11253, on the induction of OSR1$^+$ cells by the TTNPB method. (C) The knockdown efficiency of siRNAs targeting *RARB*, and (D and E) effects on expression levels of *OSR1* and the induction of OSR1$^+$ cells by the TTNPB method. (F) Effects of adding a pan-RXR agonist (SR11237) or a pan-RXR antagonist (UVI3003) to the induction efficiency of OSR1$^+$ cells by the TTNPB method. (G) The induction of OSR1$^+$ cells by the small molecule method, when SR11237 replaced AM580 or TTNPB. (H) Results of qRT-PCR analyses showing *OSR1* expression activated by the AM580 and TTNPB methods, and when ATRA, adapalene, or CD1530 were used instead of AM580 or TTNPB. OSR1-GFP knock-in hiPSCs prior to treatments were used to normalize the data. The data in (A–H) are presented as the mean±SD on culture day 6 of three independent experiments (n = 3).
doi:10.1371/journal.pone.0084881.g004

tion levels were substantially attenuated by adding noggin or DMH1 to the culture (Figure 5G).

We next assessed the efficacy of treatment with BMP-4 or BMP-5 alone for inducing OSR1$^+$ cells from hiPSCs. Induction was increased by approximately 45% after five days of treatment with 10 or 100 ng/ml BMP-4. In contrast, treatment with BMP-5 did not lead to any significant induction of OSR1$^+$ cells, and no synergistic effects of BMP-4 and BMP-5 were observed, although both BMP-4 and BMP-5 were abundantly expressed in the differentiation cultures (Figure 5H). These results indicate that BMP-4, but not BMP-5, plays a crucial role in IM differentiation from hiPSCs, and that the mechanisms underlying the small molecule method include activation of the Smad1/5 signaling pathways through increased BMP-4 expression.